Research in Diagnostic and Interventional Imaging 9 (2024) 100038

Contents lists available at ScienceDirect

Research in Diagnostic and Interventional Imaging

journal homepage: https://www.journals.elsevier.com/redii

Original article

Feasibility of deep learning-reconstructed thin-slice single-breath-hold HASTE for detecting pancreatic lesions: A comparison with two conventional T2-weighted imaging sequences

Kai Liu[a,#], Qing Li[a,#], Xingxing Wang[b], Caixia Fu[c], Haitao Sun[a,*], Caizhong Chen[a], Mengsu Zeng[a]

[a] Department of Radiology, Zhongshan Hospital, Fudan University, Shanghai Institute of Medical Imaging, Shanghai 200032, China
[b] Department of Pathology, Zhongshan Hospital, Fudan University, Shanghai 200032, China
[c] Siemens (Shenzhen) Magnetic Resonance Ltd., Shenzhen, China

ARTICLE INFO

Article History:
Received 8 July 2023
Accepted 26 December 2023
Available online 31 January 2024

Keywords:
Deep learning
Half-Fourier acquisition single-shot turbo spin echo
Pancreatic lesions
Compressed sensing

ABSTRACT

Objective: The objective of this study was to evaluate the clinical feasibility of deep learning reconstruction-accelerated thin-slice single-breath-hold half-Fourier single-shot turbo spin echo imaging ($HASTE_{DL}$) for detecting pancreatic lesions, in comparison with two conventional T2-weighted imaging sequences: compressed-sensing HASTE ($HASTE_{CS}$) and BLADE.

Methods: From March 2022 to January 2023, a total of 63 patients with suspected pancreatic-related disease underwent the $HASTE_{DL}$, $HASTE_{CS}$, and BLADE sequences were enrolled in this retrospectively study. The acquisition time, the pancreatic lesion conspicuity (LC_P), respiratory motion artifact (RMA), main pancreatic duct conspicuity (MPDC), overall image quality (OIQ), signal-to-noise ratio (SNR), and contrast-noise-ratio (CNR) of the pancreatic lesions were compared among the three sequences by two readers.

Results: The acquisition time of both $HASTE_{DL}$ and $HASTE_{CS}$ was 16 s, which was significantly shorter than that of 102 s for BLADE. In terms of qualitative parameters, Reader 1 and Reader 2 assigned significantly higher scores to the LC_P, RMA, MPDC, and OIQ for $HASTE_{DL}$ compared to $HASTE_{CS}$ and BLADE sequences; As for the quantitative parameters, the SNR values of the pancreatic head, body, tail, and lesions, the CNR of the pancreatic lesion measured by the two readers were also significantly higher for $HASTE_{DL}$ than for $HASTE_{CS}$ and BLADE sequences.

Conclusions: Compared to conventional T2WI sequences ($HASTE_{CS}$ and BLADE), deep-learning reconstructed HASTE enables thin slice and single-breath-hold acquisition with clinical acceptable image quality for detection of pancreatic lesions.

1. Introduction

Magnetic resonance imaging (MRI), with its excellent spatial resolution and absence of radiation, plays a vital role in the diagnosis of pancreatic diseases[1]. T2-weighted imaging (T2WI), including fat-suppressed T2WI, as an essential component of pancreatic MRI sequences, enabling the detection and diagnosis of pancreatic structures and lesions [2]. However, conventional T2-weighted turbo spin echo (TSE) sequences are time-consuming (several minutes) and prone to motion artifacts due to multiple breath-hold and respiratory-triggered acquisitions[3]. These motion or respiratory artifacts can undermine radiologists' confidence and accuracy in pancreatic diagnosis[4]. Furthermore, the pancreas, being thinner and surrounded by adjacent tissues, requires higher image quality compared to other abdominal organs[5,6]. Image fuzziness, misregistration, reduced signal-to-noise ratio, or contrast can obscure significant pancreatic lesions and anatomical structures.

Despite the development of additional techniques such as respiratory-triggering or k-space filling techniques, which have somewhat reduced respiratory motion artifacts, they still require long image acquisition time and multiple breath-holds[7,8]. Single-shot T2WI techniques, such as single-shot fast spin echo (single-shot FSE) and the half-Fourier acquisition single-shot turbo spin echo (HASTE), have been considered as alternatives for reduce motion artifacts due to their faster acquisition times and improved motion stability at baseline[9,10]. However, compared to conventional T2W TSE, the imaging contrast and quality in single-shot FSE T2WI techniques exhibit reduced imaging contrast and quality due to longer echo training [11]. In contrast, HASTE T2WI acquired less k-space data,

* Corresponding author.
E-mail address: sht1720@163.com (H. Sun).
# These authors contributed equally to this work.

https://doi.org/10.1016/j.redii.2023.100038

allowing for shorter scan times and further reduction of motion artifacts at the cost of reduced spatial resolution and lesion conspicuity.

More acceleration methods have been developed and applied in the clinic to obtain T2W images with shorter acquisition time and higher quality [12,13]. For example, compression sensing (CS), an acceleration technique, has been employed to achieve faster scanning with improved image quality by bypassing the Nyquist-Shannon sampling criterion and utilizing non-coherent k-space sampling[14–16]. However, despite advancements in sparse transform algorithms, the reconstruction of undamaged and clear images from randomly and highly under-sampled k-space data, and the preservation of microscopic anatomical structures, remains challenging when utilizing the CS acceleration technique. Additionally, the incorporation of trainable deep learning (DL) algorithms, such as convolutional neural networks (CNNs), into reconstruction techniques to improve the inherent defects of conventional imaging scans has been intensively developed [17,18]. For instance, in our center, several modified T2WI based on DL-based reconstruction, such as single-breath-hold T2WI and artificial intelligence-assisted compressed sensing single-shot fluid-attenuated inversion recovery, have successfully applied in the liver and brain lesion detection[19,20]. DL reconstruction-accelerated HASTE ($HASTE_{DL}$) has shown its advantages in abdominal MRI [21,22]. However, there is a lack of studies on DL techniques specifically applied to pancreas T2WI.

Therefore, the objective of our study was to evaluate the clinical feasibility of thin-slice single-breath-hold $HASTE_{DL}$ for the detection of pancreatic lesions and compare its performance with HASTE based on compressed sensing ($HASTE_{CS}$) and BLADE techniques.

2. Materials and methods

This retrospective study was approved by the Institutional Review Board of our hospital (approval no. B2020−346R), and the informed consent was waived. The process in our study strictly adheres to ethical- and hospital-related guidelines and regulations.

2.1. Participants

From March 2022 to April 2023, 63 patients with the suspected pancreatic-related disease who underwent abdominal 3T MRI were enrolled.

The inclusion criteria of this study were as follows: a) patients with radiologically assessable pancreatic lesions, with or without surgical or endoscopic puncture pathology confirmation; b) all patients with complete clinical and radiological data, including images from at least three sequences of $HASTE_{DL}$ and $HASTE_{CS}$, and BLADE. Additionally, the exclusion criteria consisted of: a) patients with claustrophobia or unable to complete the examination, b) poor image quality due to severe metallic or motion artifacts.

2.2. Image acquisition

All patients in the study underwent MRI using a 3-T MR scanner (MAGNETOM Prisma; Siemens Healthcare, Erlangen, Germany). The examination protocol consisted of conventional T1WI, diffusion-weighted imaging (DWI, b = 0, 800 s/mm^2), BLADE, and the research applications $HASTE_{DL}$ and $HASTE_{CS}$, which were randomly conducted before contrast. Then, dynamic enhanced imaging was conducted using gadolinium diethylenetriamine pentaacetic acid (Gd-DTPA, Bayer HealthCare, dose, 0.1 mmol/kg; rate, 2 mL/s). The arterial, portal, and delayed phases were obtained at 20, 90, and 180 s, respectively. In this study, the total scan time was 102 s for BLADE with four breath-holds and 16 s for both $HASTE_{DL}$ and $HASTE_{CS}$ with single breath-hold. The rest of the detailed protocols of $HASTE_{DL}$, $HASTE_{CS}$, and BLADE are listed in Table 1.

2.3. MRI image analyses

All T2WI images acquired with $HASTE_{DL}$, $HASTE_{CS}$, and BLADE were independently analyzed by two radiologists (Reader 1, X.X. X, and Reader 2, X.X.X, with 8 and 23 years of radiological experiences in pancreatic diseases, respectively) who were blinded to clinical, pathological, and radiological results during the review processing.

2.3.1. Qualitative imaging analysis

The pancreatic lesion conspicuity (LC_P), respiratory motion artifact (RMA), main pancreatic duct conspicuity (MPDC), and overall image quality (OIQ) were independently and subjective scored by three readers for three T2WI sequences. These indicators were evaluated according to a five-point Likert scale as follows: 1 (severe): the presence of blurry edges of pancreatic lesions or structures, heavy image artifacts, and poor image continuity that do not meet the diagnostic requirements; 2 (moderate): the presence of relatively blurry edges of pancreatic lesions or structures, heavy image artifacts, and poor image continuity

Table 1
Different s sequences protocols.

	$HASTE_{DL}$	$HASTE_{CS}$	BLADE
TR (ms)	628	628	3000
TE (ms)	105	105	114
Matrix	320×320	320×320	320×320
Field of view (mm^2)	360×360	360×360	360×360
Voxel size (mm^3)	1.1 × 1.1 × 4	1.1 × 1.1 × 4	1.1 × 1.1 × 4
Section thickness (mm)	4	4	4
Slice gap (mm)	0.4	0.4	0.4
Number of sections	26	26	26
Flip angle (°)	130	130	120
Bandwidth (Hz)	710	710	600
Acceleration	3.3	3.3	2
Respiratory control	single breath-hold	single breath-hold	four breath-holds
Single breath-hold time (s)	16	16	18
Fat suppression	SPAIR	SPAIR	SPAIR
TA (s)	16	16	102

TR, Repetition time; TE, Echo time; PAT, parallel acquisition technique; SPAIR, spectral-attenuated inversion recovery; TA, acquisition time.

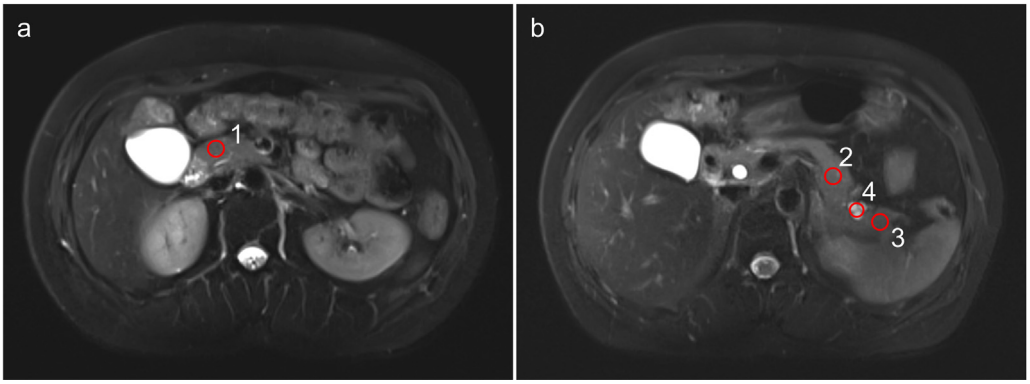

Fig. 1. Representative ROI placement for the head (1), body (2), tail (3), and lesion (4) of the pancreas.

that make it difficult to meet the diagnostic requirements; 3 (mild): the presence of slightly blurry edges of pancreatic lesions or structure, and acceptable image artifacts and continuity that meet the basic diagnostic requirements. 4 (fine): the presence of relatively sharp and clear edges of pancreatic lesions or structure, and negligible image artifacts and continuity that meet the diagnostic requirements; 5 (excellent): pancreatic lesions or structures with completely sharp and clear edges, no image artifacts, good continuity, and fully compliant with diagnostic requirements. Moreover, slice continuity, defined as inconsistent horizontal position between layers, was divided into discontinuity or no discontinuity. The above two radiologists analyzed the slice continuity independently. When inconsistencies arose, a third radiologist with 25 years of radiological experience was asked to evaluate and use the unified opinion for follow-up analysis.

2.3.2. Quantitative image analysis

The signal intensities (SI) of the head (H), body (B), tail (T), and lesion (L) of the pancreas and the SI of the erector spinal muscle (ESM) were measured on operator-defined regions-of-interest (ROI) on the three T2WI images, respectively (Fig. 1). The sizes of ROI in the vertical spine muscle and pancreatic tissue and lesions are about 50∼100 mm^2, and the corresponding ROI is placed in the signal uniformity area, avoiding the influence of blood vessels and bones. The image signal-to-noise ratio (SNR) and contrast-to-noise ratio (CNR) are calculated according to the following formulas:

SNR of pancreatic head: $SNR_H = SI_H / SI_{ESM}$;
SNR of pancreatic body: $SNR_B = SI_B / SI_{ESM}$;
SNR of pancreatic tail: $SNR_T = SI_T / SI_{ESM}$;
SNR of pancreatic lesions: $SNR_L = SI_L / SI_{ESM}$;
CNR of pancreatic lesions: $CNR_L = |SI_L - SI_{ESM}| / SI_{ESM}$

2.4. Statistical analysis

Statistical analyses were performed using SPSS version 26 (IBM Corp., Armonk, NY, USA). The image quality scores obtained for three T2WI sequences were compared using a paired Wilcoxon signed-rank test. $P < 0.05$ was considered as statistically significant and Bonferroni correction was conducted to correct for cumulative α error [23]. Interobserver agreement was assessed using the Cohen κ coefficient [24]. The κ values were used to interpret according to the following criteria: poor (0–0.20), fair (0.21–0.40), moderate (0.41–0.60), good (0.61–0.80), almost perfect (0.81–1).

3. Results

3.1. Patient characteristics

A total of 63 patients (mean age, 61.13 ± 11.25 years; range, 30–83 years, 34 men and 29 women;) with pancreatic lesions were enrolled in the present study for subsequent analysis.

Regarding pancreatic lesions, surgical tumor resection with pathological confirmation was performed on 31 patients. Among them, 23 patients were diagnosed with pancreatic ductal adenocarcinoma (PDAC), while 8 patients had pancreatic neuroendocrine tumors (G1, $n = 2$ and G2, $n = 6$). Additionally, 11 patients received pathologically confirmed through endoscopic puncture and were diagnosed PDAC. The remaining patients were diagnosed based on the indications of abdominal MRI and clinical signs and symptoms, including pancreatic solid tumor ($n = 7$), pancreatic cystic lesions ($n = 12$) and suspected pancreatic inflammatory disease ($n = 2$). The size of the lesions (maximum diameter) ranged from 1.1 to 7.1 cm, with a mean of (2.9 ± 1.4) cm. For the location of pancreatic lesions, there were 36 in the head of pancreas, 12 in the body of pancreas, and 19 in the tail of pancreas. Moreover, 11 cases (17.5 %) in $HASTE_{DL}$ showed slice discontinuities, significantly less than 18 (28.6 %) and 20 (31.7 %) cases in $HASTE_{CS}$ and BLADE.

3.2. Qualitative imaging analysis

The three T2WI protocols were successfully examined and analyzed in all patients. The acquisition time (AT) for both $HASTE_{DL}$ and $HASTE_{CS}$ was 16 s, while the AT for BLADE was 102 s.

The five-point Likert scale was used to assess four qualitative image qualities (LC_P, RMA, MPDC and OIQ) for $HASTE_{DL}$, $HASTE_{CS}$, and BLADE sequences (Tables 2 and 4). In terms of pancreatic lesion analysis, a total of 65 pancreatic lesions were detected and evaluated. The LC_P, RMA, and OIQ scores of $HASTE_{DL}$ in Reader 1 and Reader 2 were all significantly higher than those for $HASTE_{CS}$ and BLADE sequences (P value ranging from <0.001 to 0.003) (Figs. 2 and 3). However, there were no statistical differences in these scores between $HASTE_{CS}$ and BLADE. For pancreatic ducts, $HASTE_{DL}$ achieved highest MPDC scores of 4.67±0.48 and 4.68±0.47 in reader 1 and reader 2, respectively, which were significantly higher than those of $HASTE_{CS}$ and BLADE (P value ranging <0.001 to 0.006) (Fig. 4). In terms of MPDC, the scores for $HASTE_{CS}$ in both Reader 1 and Reader 2 were 4.48±0.59 and 4.49±0.56, respectively, which were higher than those of BLADE.

The interobserver agreement of the qualitative parameters was good to almost perfect for $HASTE_{DL}$ ($k = 0.817–0.892$), $HASTE_{CS}$ ($k = 0.763–0.917$), BLADE ($k = 0.844–0.930$).

Table 2
The qualitative parameters among $HASTE_{DL}$, $HASTE_{CS}$ and BLADE with kappa values.

	Reader 1			Reader 2			Kappa[a]	Kappa[b]	Kappa[c]
	$HASTE_{DL}$	$HASTE_{CS}$	BLADE	$HASTE_{DL}$	$HASTE_{CS}$	BLADE	$HASTE_{DL}$	$HASTE_{CS}$	BLADE
LC_P	4.60±0.43	4.02±0.66	4.05±0.88	4.75±0.44	4.00±0.65	4.03±0.89	0.872	0.917	0.930
MPDC	4.67±0.48	4.48±0.59	3.90±0.78	4.68±0.47	4.49±0.56	3.89±0.74	0.892	0.814	0.866
RMA	4.79±0.41	4.49±0.59	4.48±0.73	4.76±0.43	4.48±0.64	4.44±0.78	0.817	0.855	0.885
OIQ	4.63±0.49	4.02±0.46	3.89±0.81	4.62±0.49	3.97±0.51	3.83±0.75	0.831	0.763	0.844

LC_P: pancreatic lesion conspicuity; RM: respiratory motion artifact; MPDC: main pancreatic duct conspicuity; OIQ: overall image quality; [a] Inter-reader agreement for $HASTE_{DL}$ image was evaluated by using Cohen's kappa; [b] Inter-reader agreement for $HASTE_{CS}$ image was evaluated by using Cohen's kappa; [c] Inter-reader agreement for BLADE image was evaluated by using Cohen's kappa;.

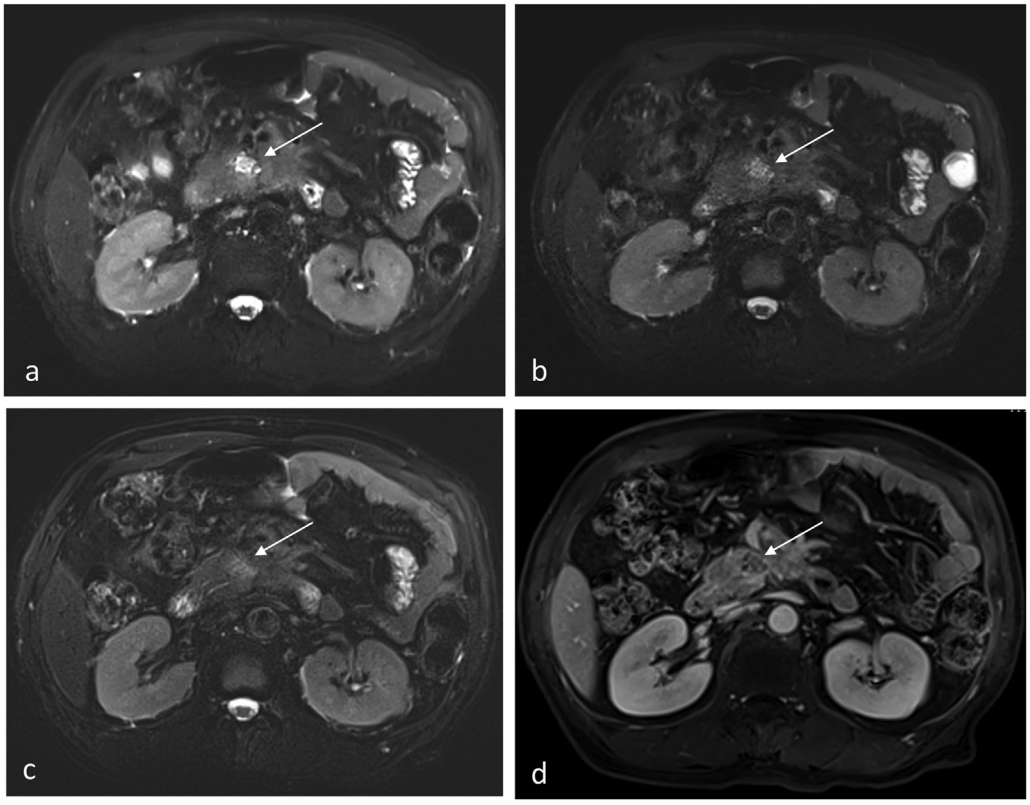

Fig. 2. A 66-year-old male with a pancreatic head tumor. The pancreas and pancreatic lesion (the arrow) can be clearly shown in $HASTE_{DL}$ (a). $HASTE_{CS}$ (b) also showed the pancreas and pancreatic lesion (the arrow); however, the contrast between lesion and the pancreas was slightly poor. The lesion shape displayed in BLADE sequence (c) is fuzzy, and the contrast is poor; The contrast-enhanced T1WI sequence (d), the gold standard for diagnosis (the portal phase), shows the pancreatic head tumor (the arrow).

3.3. Quantitative image analysis

In terms of the anatomical structures of the pancreas, the SNR_H, SNR_B, and SNR_T values measured by both two readers were highest for $HASTE_{DL}$, followed by $HASTE_{CS}$ and BLADE; and these differences were statistically significant (Tables 3 and 4). Regarding to pancreatic lesions, CNR_L and SNR_L for $HASTE_{DL}$ in both readers were higher compared to $HASTE_{CS}$ and BLADE.

The interobserver agreement for the quantitative parameters was good to almost perfect for $HASTE_{DL}$ (ICC = 0.799−0.893), $HASTE_{CS}$ (ICC = 0.825−0.882), BLADE (ICC = 0.755−889) (Table 3).

4. Discussion

In the present study, the feasibility of thin-slice single-breath-hold T2W HASTE with deep-learning-based reconstruction for detecting pancreatic lesions was investigated compared to BLADE and $HASTE_{CS}$. As results, the qualitative analyses demonstrated that the $HASTE_{DL}$ sequence exhibited improved pancreatic lesion conspicuity, main pancreatic duct conspicuity, overall image quality and less respiratory motion artifact compared to $HASTE_{CS}$ and BLADE sequences. Regarding quantitative analyses, the $HASTE_{DL}$ sequence outperformed the other two sequences in term of SNR and CNR for both pancreatic structures and lesions.

The T2WI sequence plays a crucial role in the diagnosing and exploring pancreatic diseases [25]. Compared to other abdominal organs, the pancreas is relatively thin, located deeper in the body, and more susceptible to respiratory motion artifacts, therefore, fast thin-slice T2WI scanning is preferred for detecting pancreatic disease. Although thin-slice scan allows for higher spatial resolution, it can lead to a reduction in proton signal and SNR [26,27]. Therefore, effectively reducing acquisition time and minimizing the effects of motion artifacts and thin-slice scans are critical challenges in pancreatic T2WI imaging. In our study, both the $HASTE_{DL}$ and $HASTE_{CS}$

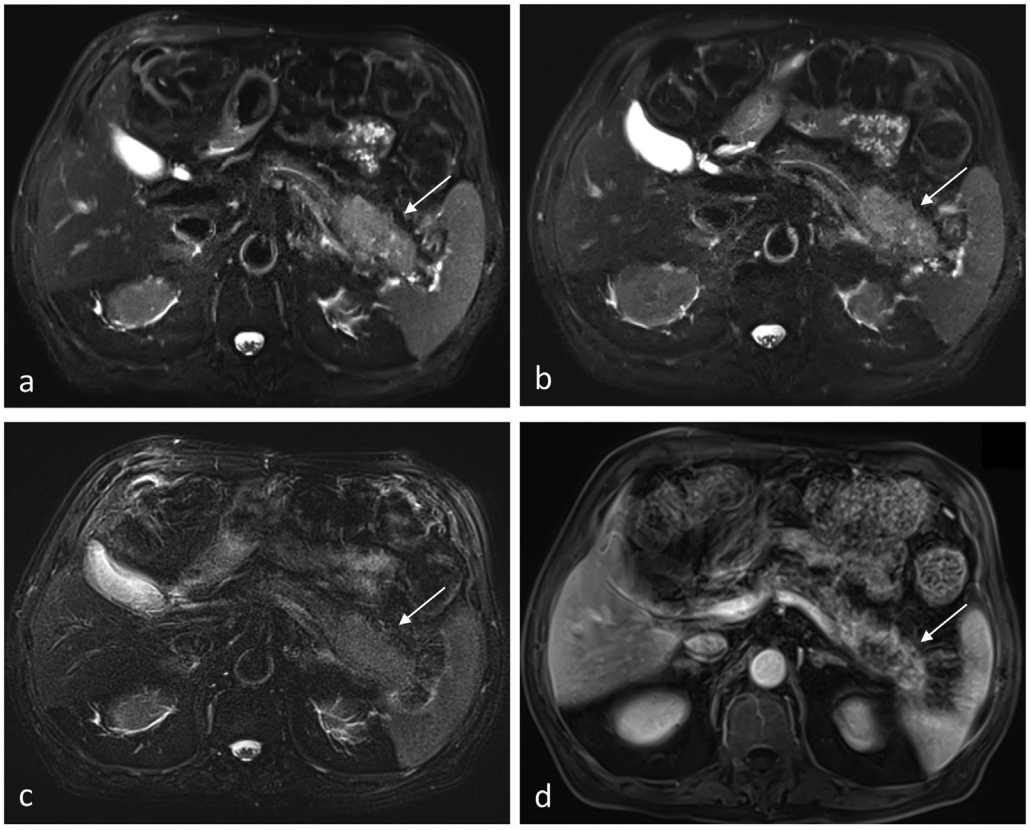

Fig. 3. An 80-year-old male with pancreatic ductal adenocarcinoma in the tail of pancreas. The pancreas and pancreatic lesion (the arrow) can be clearly shown in $HASTE_{DL}$ (a) with low noise and high SNR, significantly better than those in $HASTE_{CS}$ (b) and BLADE (c); The contrast-enhanced T1WI sequence (d), the gold standard for diagnosis (the portal phase), shows the pancreatic lesion (the arrow).

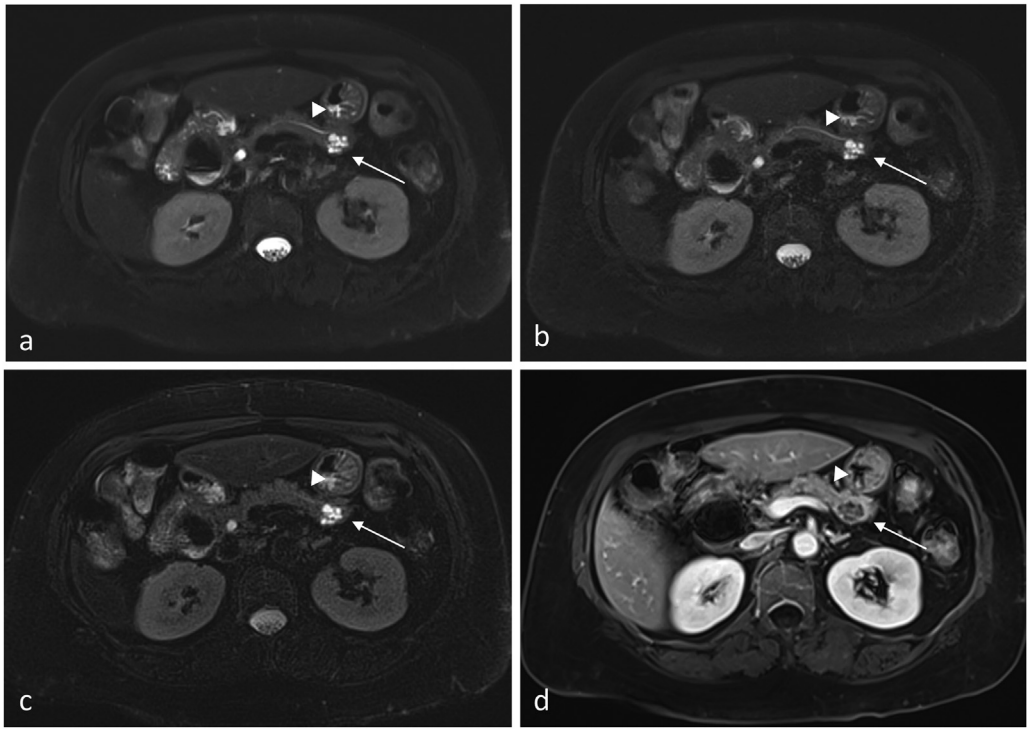

Fig. 4. A 71-year-old female with cystic lesions of the tail of the pancreas. The pancreas and pancreatic lesion (the arrow) can be clearly shown in $HASTE_{DL}$ (a), $HASTE_{CS}$ (b), and BLADE (c); Peripancreatic regional SNR performed best in $HASTE_{DL}$, but the noise around the pancreas is higher in $HASTE_{CS}$ and BLADE, decreasing the peripancreatic regional SNRs; Pancreatic duct (the triangular arrow) showed well in $HASTE_{DL}$ and $HASTE_{CS}$; however, BLADE offers poorly for the pancreatic duct; The contrast-enhanced T1WI sequence (d), the gold standard for diagnosis (the portal phase), shows the pancreatic lesion (the arrow).

Table 3
The quantitative parameters among $HASTE_{DL}$, $HASTE_{CS}$ and BLADE with ICC values.

	Reader 1 $HASTE_{DL}$	$HASTE_{CS}$	BLADE	Reader 2 $HASTE_{DL}$	$HASTE_{CS}$	BLADE	ICC[a] $HASTE_{DL}$	ICC[b] $HASTE_{CS}$	ICC[c] BLADE
SNR_H	39.17±44.44	36.97±51.63	14.98±12.12	43.09±37.92	35.15±46.70	16.11±11.73	0.876	0.882	0.889
SNR_B	37.66±43.06	35.91±51.27	14.78±12.66	41.94±46.97	32.59±46.16	16.09±14.03	0.891	0.850	0.757
SNR_T	37.00±43.92	34.47±48.61	12.78±11.00	39.35±53.31	36.40±57.94	13.78±13.52	0.799	0.861	0.828
SNR_L	90.62±103.74	83.74±128.75	34.52±25.64	102.17±108.50	89.34±131.22	39.01±39.74	0.893	0.825	0.755
CNR_L	73.83±99.32	54.11±76.59	33.72±39.01	79.07±93.30	52.88±64.05	35.40±31.74	0.892	0.841	0.783

ICC, intraclass correlation; SNR_H: SNR of pancreatic head; SNR_B: SNR of pancreatic body; SNR_T: SNR of pancreatic tail; SNR_L: SNR of pancreatic lesions; CNR_L: CNR of pancreatic lesions; [a] Inter-reader agreement for $HASTE_{DL}$ image was evaluated by using ICC; [b] Inter-reader agreement for $HASTE_{CS}$ image was evaluated by using ICC; [c] Inter-reader agreement for BLADE image was evaluated by using ICC.

Table 4
The comparisons of qualitative and quantitative parameters among $HASTE_{DL}$, $HASTE_{CS}$ and BLADE.

Imaging quality	Reader 1 P_{DLvsCS}	P_{DLvsBL}	P_{CSvsBL}	Reader 2 P_{DLvsCS}	P_{DLvsBL}	P_{CSvsBL}
LC_P	<0.001	<0.001	0.809	<0.001	<0.001	0.809
MPDC	0.006	<0.001	<0.001	0.004	<0.001	<0.001
RMA	<0.001	0.002	0.834	0.001	0.003	0.582
OIQ	<0.001	<0.001	0.185	<0.001	<0.001	0.129
SNR_H	<0.001	<0.001	<0.001	<0.001	<0.001	<0.001
SNR_B	<0.001	<0.001	<0.001	<0.001	<0.001	<0.001
SNR_T	<0.001	<0.001	<0.001	<0.001	<0.001	<0.001
SNR_L	<0.001	<0.001	<0.001	<0.001	<0.001	<0.001
CNR_L	<0.001	<0.001	<0.001	<0.001	<0.001	<0.001

LC_P: pancreatic lesion conspicuity; RMA: respiratory motion artifact; SNR_H: SNR of pancreatic head; SNR_B: SNR of pancreatic body; SNR_T: SNR of pancreatic tail; SNR_L: SNR of pancreatic lesions; CNR_L: CNR of pancreatic lesions; MPDC: main pancreatic duct conspicuity; OIQ: overall image quality; P value less than 0.017 after Bonferroni correction are statistical significance.

sequences were able to complete a single breath-hold scan in 16 s. In contrast, the conventional BLADE sequence requires multiple breath-holds and had an acquisition time of 106 s, significantly increasing the time and cost required for routine clinical examinations.

The irregular morphology of the pancreas, its narrow alignment, and its central location within the abdomen make it more challenging to obtain clear images with clinically acceptable SNR compared to organs such as the liver closer to the coils [26]. Regarding the conspicuity of the pancreatic duct and lesions, $HASTE_{DL}$ was significantly preferred over the other two sequences, resulting in a substantial improvement in diagnostician confidence. Furthermore, the $HASTE_{DL}$ sequence demonstrated distinct advantages in suppressing respiratory artifacts and enhancing overall image quality. The conventional BLADE technique was initially developed to reduce motion artifacts in T2WI. However, the acquisition time of the BLADE sequence remains long. In our study, the acquisition time of BLADE was approximately six times higher than the other two sequences. While respiratory-triggered sampling methods theoretically allow for obtaining high-quality images, the effectiveness and image quality heavily rely on the patient's respiratory rhythm and amplitude. Unfortunately, most patients with pancreatic disease struggle to maintain a consistent and regular respiratory rhythm, resulting in variable acquisition times ranging from approximately 2 to 6 min. An additional concern is that when a patient's respiratory rhythm is unstable, techniques reliant on respiratory triggering may still produce respiratory artifacts and misaligned images, posing a particular risk for the inherently thin pancreas. This can increase the likelihood of losing images of the pancreatic lesion, thereby reducing diagnostic confidence.

DL has made significant advancements in recent years, integrating trainable deep learning algorithms into reconstruction techniques[28–30]. This integration addresses the limitations of conventional imaging scans and has been extensively developed for clinical applications [31]. DL reconstruction methods have demonstrated the ability to effectively reduce imaging noise while preserving image resolution[22,32] . In our present study, we employed regular under-sampling without integrated reference data in our thin-slice single-breath-hold HASTE T2WI, using a DL-based reconstruction approach. This approach aimed to shorten the echo train time and reduce the specific absorption rate, while reference data was obtained using a smaller flip angle, effectively reducing the specific absorption rate. Additionally, we incorporated variational networks that included bias-field correction and coil-sensitivity maps, along with iterations and trainable extrapolation steps. These techniques allowed for acquisitions without integrated calibration and offered flexibility in k-space sampling. Furthermore, to improve image quality, we utilized a residual dense U-net as image regularization [21]. The introduction of DL in HASTE retains its fundamental advantages of fast imaging and motion artifact reduction while significantly reducing noise and enhancing image resolution.

In our study, we also explored the application of CS for HASTE sequences in pancreas T2WI. CS-accelerated T2WI has gained popularity in the examination of abdominal organs, particularly the liver [33]. Previous studies on liver imaging have demonstrated that multiple breath-hold $HASTE_{CS}$ sequences improve the signal-to-noise ratio and image quality compared to conventional multiple breath-hold T2WI [33]. Unfortunately, there is limited research comparing CS-accelerated T2WI and DL-accelerated T2WI imaging for pancreatic diseases [34]. We observed that the $HASTE_{CS}$ sequences exhibited improved signal-to-noise ratio compared to BALDE. However, there was no significant difference in the objective evaluation of image quality. Regrettably, the CS-accelerated $HASTE_{CS}$ sequence resulted in increased image noise, and the combination of high under-sampling and thin-slice scanning further exacerbated the reduced SNR of the

images. The image SNR, image quality, and lesion visualization in $HASTE_{CS}$ were inferior to those of $HASTE_{DL}$. Theoretical analysis suggests that $HASTE_{CS}$ struggles to reconstruct uncorrupted images from randomly and highly under-sampled k-space data or microanatomical structures, due to the limitations of sparse transform algorithms [35]. Additionally, compared to DL algorithms, the typical regularization and iterative optimization algorithms used in CS are simple and crude, lacking the trainability offered by DL. Considering the overall image quality and acquisition time, the single breath-hold $HASTE_{DL}$ demonstrated better application and robustness in fast thin-slice T2W imaging for the detection of pancreatic lesions.

However, there are several limitations in our study. Firstly, although we included a wide range of patients with various pancreatic diseases including tumors or inflammation, the sample size was relatively small which may introduce selection bias to some extent. Secondly, due to the timing and nature of the experiment, we were unable to obtain pathological results for a proportion of patients diagnosed with benign tumors or inflammatory lesions. Instead, their diagnoses relied on clinical, radiological and laboratory findings.

In conclusion, the thin-slice single-breath-hold $HASTE_{DL}$ demonstrates promising capability, providing significantly superior image quality and SNR for pancreatic lesions, compared with compared to $HASTE_{CS}$ and BLADE. Moreover, $HASTE_{DL}$ exhibits excellent pancreatic lesion conspicuity and contrast, leading to increased diagnostic confidence among radiologists. Considering acquisition time and overall image qualities, $HASTE_{DL}$ could potentially become a standard protocol for thin-slice pancreatic MRI and may substitute conventional T2WI sequences.

Author contribution

All authors attest that they meet the current International Committee of Medical Journal Editors (ICMJE) criteria for authorship. The author(s) declare(s) that they had full access to all of the data in this study and the author(s) take(s) complete responsibility for the integrity of the data and the accuracy of the data analysis.

Declaration of competing interest

The authors declare the following financial interests/personal relationships which may be considered as potential competing interests:

Haitao Sun reports a relationship with Zhongshan Hospital Fudan University that includes: non-financial support.

Funding

This project was funded by "Science and Technology Innovation Action Plan" Star Cultivation (Sailing Program) (22YF1443600) and the China Postdoctoral Science Foundation (2023M732230).

Ethical approval

All procedures performed in studies involving human participants were in accordance with the ethical standards of the institutional and/or national research committee and with the 1964 Helsinki declaration and its later amendments or comparable ethical standards.

References

[1] Chu LC, Goggins MG, Fishman EK. Diagnosis and detection of pancreatic cancer. Cancer J 2017;23:333–42. doi: 10.1097/PPO.0000000000000290.
[2] Zhang BB, Hou XM, Chen YQ, Huo JW, Jin EH. Imaging features and risk factors of pancreatic cystic lesions complicating autoimmune pancreatitis: a retrospective study. Curr Med Imaging 2023. doi: 10.2174/1573405619666230314095508.
[3] Glaser C, D'Anastasi M, Theisen D, Notohamiprodjo M, Horger W, Paul D, et al. Understanding 3d tse sequences: advantages, disadvantages, and application in MSK imaging. Semin Musculoskelet Radiol 2015;19:321–7. doi: 10.1055/s-0035-1563732.
[4] Kabasawa H, Kiryu S. Pulse sequences and reconstruction in fast mr imaging of the liver. Magn Reson Med Sci 2023;22:176–90. doi: 10.2463/mrms.rev.2022-0114.
[5] Chang H, Bates D, Gupta A, LeBedis CA. Use of MR in pancreaticobiliary emergencies. Magn Reson Imaging Clin N Am 2022;30:479–99. doi: 10.1016/j.mric.2022.04.009.
[6] Briola C. Magnetic resonance imaging and magnetic resonance imaging cholangiopancreatography of the pancreas in small animals. Vet Sci 2022;9. doi: 10.3390/vetsci9080378.
[7] Kraus MS, Coblentz AC, Deshpande VS, Peeters JM, Itriago-Leon PM, Chavhan GB. State-of-the-art magnetic resonance imaging sequences for pediatric body imaging. Pediatr Radiol 2022. doi: 10.1007/s00247-022-05528-y.
[8] Chhetri A, Li X, Rispoli JV. Current and emerging magnetic resonance-based techniques for breast cancer. Front Med 2020;7:175. doi: 10.3389/fmed.2020.00175.
[9] Tyrell D, Mohamed F, Pavlides C, Kutalek S, Mulhern C, Nunes LW. Half-fourier acquisition single-shot turbo spin echo imaging in the diagnosis of morgagni hernia. J Magn Reson Imaging 2001;14:653–7. doi: 10.1002/jmri.1231.
[10] Castillo M, Mukherji SK. Clinical applications of flair, haste, and magnetization transfer in neuroimaging. Semin Ultrasound Ct Mr 2000;21:417–27. doi: 10.1016/s0887-2171(00)90034-9.
[11] Kabakus IM, Spampinato MV, Knipfing M, Cervantes G, Patel A, Eskandari R, et al. Fast brain magnetic resonance imaging with half-fourier acquisition with single-shot turbo spin echo sequence in detection of intracranial hemorrhage and skull fracture in general pediatric patients: preliminary results. Pediatr Emerg Care 2021;37:e1168–72. doi: 10.1097/PEC.0000000000001949.
[12] Rajiah PS, François CJ, Leiner T. Cardiac MRI: state of the art. Radiology 2023;307:e223008. doi: 10.1148/radiol.223008.
[13] Zibetti M, Menon RG, de Moura HL, Zhang X, Kijowski R, Regatte RR. Updates on compositional MRI mapping of the cartilage: emerging techniques and applications. J Magn Reson Imaging 2023. doi: 10.1002/jmri.28689.
[14] Taron J, Weiss J, Notohamiprodjo M, Kuestner T, Bamberg F, Weiland E, et al. Acceleration of magnetic resonance cholangiopancreatography using compressed sensing at 1.5 and 3 t. Invest Radiol 2018;53:681–8. doi: 10.1097/RLI.0000000000000489.
[15] Zhu L, Xue H, Sun Z, Qian T, Weiland E, Kuehn B, et al. Modified breath-hold compressed-sensing 3D MR cholangiopancreatography with a small field-of-view and high resolution acquisition: clinical feasibility in biliary and pancreatic disorders. J Magn Reson Imaging 2018;48:1389–99. doi: 10.1002/jmri.26049.
[16] Hausmann D, Niemann T, Kreul D, Nocito A, Klarhöfer M, Nickel DM, et al. Free-breathing dynamic contrast-enhanced imaging of the upper abdomen using a cartesian compressed-sensing sequence with hard-gated and motion-state-resolved reconstruction. Invest Radiol 2019;54:728–36. doi: 10.1097/RLI.0000000000000607.
[17] Hu F, Chen AA, Horng H, Bashyam V, Davatzikos C, Alexander-Bloch A, et al. Image harmonization: a review of statistical and deep learning methods for removing batch effects and evaluation metrics for effective harmonization. Neuroimage 2023;274:120125. doi: 10.1016/j.neuroimage.2023.120125.
[18] Berbís MA, Paulano GF, Royuela DVJ, Alcalá ML, Luna A. Clinical impact of artificial intelligence-based solutions on imaging of the pancreas and liver. World J Gastroenterol 2023;29:1427–45. doi: 10.3748/wjg.v29.i9.1427.
[19] Sheng R, Zheng L, Jin K, Sun W, Liao S, Zeng M, et al. Single-breath-hold T2WI liver MRI with deep learning-based reconstruction: a clinical feasibility study in comparison to conventional multi-breath-hold T2WI liver MRI. Magn Reson Imaging 2021;81:75–81. doi: 10.1016/j.mri.2021.06.014.
[20] Liu K, Xi B, Sun H, Wang J, Chen C, Wen X, et al. The clinical feasibility of artificial intelligence-assisted compressed sensing single-shot fluid-attenuated inversion recovery (acs-ss-flair) for evaluation of uncooperative patients with brain diseases: comparison with the conventional t2-flair with parallel imaging. Acta Radiol 2023;64:1943–9. doi: 10.1177/02841851221139125.
[21] Herrmann J, Nickel D, Mugler JP, Arberet S, Gassenmaier S, Afat S, et al. Development and evaluation of deep learning-accelerated single-breath-hold abdominal haste at 3 t using variable refocusing flip angles. Invest Radiol 2021;56:645–52. doi: 10.1097/RLI.0000000000000785.
[22] Herrmann J, Gassenmaier S, Nickel D, Arberet S, Afat S, Lingg A, et al. Diagnostic confidence and feasibility of a deep learning accelerated haste sequence of the abdomen in a single breath-hold. Invest Radiol 2021;56:313–9. doi: 10.1097/RLI.0000000000000743.
[23] Yu M, Tang X, Jin H, Yang S, Yun H, Wang Q, et al. Coronary ct angiography in asymptomatic adults with hepatic steatosis. Radiology 2021;301:593–601. doi: 10.1148/radiol.2021210355.
[24] Chen Z, Xue Y, Wu Y, Duan Q, Zheng E, He Y, et al. Feasibility of 3d breath-hold mr cholangiopancreatography with a spatially selective radiofrequency excitation pulse: prospective comparison with parallel imaging technique and compressed sensing method. Acad Radiol 2022;29:e289–95. doi: 10.1016/j.acra.2022.03.006.
[25] Song Q, Shi Y, Gao F, Yin M, Yang R, Liu Y, et al. Feasibility and reproducibility of multifrequency magnetic resonance elastography in healthy and diseased pancreases. J Magn Reson Imaging 2022;56:1769–80. doi: 10.1002/jmri.28158.
[26] Tajima T, Akai H, Yasaka K, Kunimatsu A, Akahane M, Yoshioka N, et al. Clinical feasibility of an abdominal thin-slice breath-hold single-shot fast spin echo sequence processed using a deep learning-based noise-reduction approach. Magn Reson Imaging 2022;90:76–83. doi: 10.1016/j.mri.2022.04.005.
[27] Hong GS, Byun JH, Kim JH, Kim HJ, Lee SS, Hong SM, et al. Thread sign in biliary intraductal papillary mucinous neoplasm: a novel specific finding for mri. Eur Radiol 2016;26:3112–20. doi: 10.1007/s00330-015-4158-5.

[28] Njølstad T, Schulz A, Jensen K, Andersen HK, Martinsen ACT. Improved image quality with deep learning reconstruction – a study on a semi-anthropomorphic upper-abdomen phantom. ReDII 2023;5:100022. doi: 10.1016/j.redii.2023.100022.
[29] Chaika M, Afat S, Wessling D, Afat C, Nickel D, Kannengiesser S, et al. Deep learning-based super-resolution gradient echo imaging of the pancreas: improvement of image quality and reduction of acquisition time. Diagn Interv Imaging 2023;104:53–9. doi: 10.1016/j.diii.2022.06.006.
[30] Ahmed TM, Kawamoto S, Hruban RH, Fishman EK, Soyer P, Chu LC. A primer on artificial intelligence in pancreatic imaging. Diagn Interv Imaging 2023;104:435–47. doi: 10.1016/j.diii.2023.03.002.
[31] Aggarwal HK, Mani MP, Jacob M. Modl: model-based deep learning architecture for inverse problems. IEEE Trans Med Imaging 2019;38:394–405. doi: 10.1109/TMI.2018.2865356.
[32] Zhou Z, Han F, Ghodrati V, Gao Y, Yin W, Yang Y, et al. Parallel imaging and convolutional neural network combined fast MR image reconstruction: applications in low-latency accelerated real-time imaging. Medical Physics 2019;46:3399–413. doi: 10.1002/mp.13628.
[33] Sun W, Wang W, Zhu K, Chen C, Wen X, Zeng M, et al. Feasibility of compressed sensing technique for isotropic dynamic contrast-enhanced liver magnetic resonance imaging. Eur J Radiol 2021;139:109729. doi: 10.1016/j.ejrad.2021.109729.
[34] Han S, Lee JM, Kim SW, Park S, Nickel MD, Yoon JH. Evaluation of haste T2 weighted image with reduced echo time for detecting focal liver lesions in patients at risk of developing hepatocellular carcinoma. Eur J Radiol 2022;157:110588. doi: 10.1016/j.ejrad.2022.110588.
[35] Kromrey M, Funayama S, Tamada D, Ichikawa S, Shimizu T, Onishi H, et al. Clinical evaluation of respiratory-triggered 3d mrcp with navigator echoes compared to breath-hold acquisition using compressed sensing and/or parallel imaging. Magn Reson Med Sci 2020;19:318–23. doi: 10.2463/mrms.mp-2019-0122.